Helium Tunneling through Nitrogen-Functionalized Graphene Pores: Pressure-and Temperature-Driven Approaches to Isotope Separation

3 AUTHORS:

Andreas W Hauser
Graz University of Technology
34 PUBLICATIONS **396** CITATIONS

SEE PROFILE

Joshua Schrier
Haverford College
48 PUBLICATIONS **1,023** CITATIONS

SEE PROFILE

Peter Schwerdtfeger
Massey University
339 PUBLICATIONS **8,300** CITATIONS

SEE PROFILE

Helium Tunneling through Nitrogen-Functionalized Graphene Pores: Pressure- and Temperature-Driven Approaches to Isotope Separation

Andreas W. Hauser,*,[†] Joshua Schrier,*,[‡] and Peter Schwerdtfeger*,[†,§]

[†]Centre for Theoretical Chemistry and Physics (CTCP), The New Zealand Institute for Advanced Study (NZIAS), Massey University (Auckland Campus), Private Bag 102904, North Shore City, 0745 Auckland, New Zealand

[‡]Department of Chemistry, Haverford College, Haverford, Pennsylvania 19041, United States

[§]Fachbereich Chemie, Philipps-Universität Marburg, Hans-Meerwein-Straße, 35032 Marburg, Germany

S *Supporting Information*

ABSTRACT: Recently, we showed that nitrogen-functionalized nanopores obtained by removing two rings from a perfect graphene sheet provide suitable barriers for a separation of fermionic helium-3 from its bosonic counterpart helium-4 [*J. Phys. Chem. Lett.* 2012, 3, 209−213]. In this follow-up Article, we provide potential curves for helium passing through several different types of pores, discuss the relation of the barrier height to the effective pore size, give estimations for bound states of helium attached to the pores, and analyze the effects of isomeric and stoichiometric variations of the pore-rim nitrogen-passivation on the gas separation performance. Slight deviations in the tunneling probability for the two helium isotopes can lead to a high selectivity at an industrially acceptable gas flux if the gas temperature is kept sufficiently low. We also recently showed that the mass-dependence of quantum tunneling and zero-point energy differences at the top of the potential energy barrier allow for a classically prohibited steady-state thermally driven isotope separation [*Chem. Phys. Lett.* 2012, 521, 118−124]. The nitrogen-passivated nanopores studied here give rise to larger steady-state isotopic enrichment than that in previous work and are dominated by zero-point energy differences at both high and low temperatures.
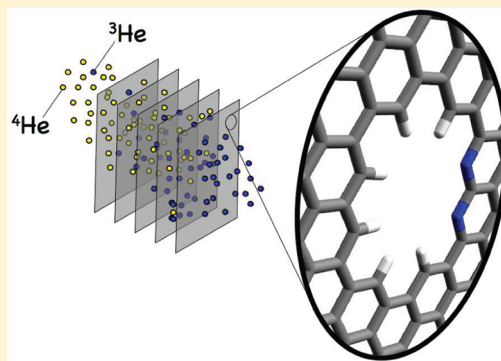
1. INTRODUCTION

The growing demand for ³He, a very rare and hence highly precious gas that is usually obtained as a byproduct of the radioactive decay of tritium, led to a critical situation for low temperature research institutes and cryogenic industries.[1] An imbalance of supply and demand is already affecting fundamental research in ultracold physics and chemistry, where ³He is mainly used in dilution refrigerators. In a recent Letter, we showed that a new type of nanoporous graphene could be used to harvest ³He directly from terrestrial helium sources.[2] In this Article, we present a more comprehensive, extended study and discuss our results in greater detail. We analyze the suggested strategy of pore size enlargement, a combination of ring removal and nitrogen passivation, for a larger set of different pore models, calculate bound states of helium atoms in these pores, and discuss the more realistic case of a pore size distribution for the most effective pore type.

With the isolation of a free-standing single graphene sheet in 2004,[3] a whole new branch of materials science evolved and led to new insights in physics, chemistry, and the applied sciences.[4−9] The impermeability and essentially two-dimensional structure of graphene make it a perfect gas separation membrane material. The chemically inert surface of a pure graphene sheet is impermeable even to helium atoms, which are repelled by the electron density of the aromatic rings.[10] A barrier height of 11.67 eV is reported for He escaping through a nondefect graphene sheet.[11] Hence, the introduction of nanosized holes with appropriate rim passivation and diameter is necessary to allow for gas transport. Common techniques are electron beam treatment or the design of suitable precursors for the self-assembling of porous graphene structures.[12,13] Although not yet realized in a suitable size and quality, the possibility of producing nanoporous graphene with ordered arrays of monodisperse pores has motivated several studies on pore design for applications such as the separation of hydrogen from methane,[14−17] the separation of helium from other noble gases and methane,[16,18] the selective passage of ions,[19] the characterization of DNA,[20] and the filtration of water.[21] Recently, asymmetrically decorated, doped graphene pores have been suggested for hydrogen isotope separation.[22]

Here, we focus on the development of a functionalized pore type for the separation of ³He from ⁴He. We first described the use of the mass-dependence of tunneling through nanoporous graphene for He isotope separation in ref 18. However, the

large barrier height associated with that structure necessitated high temperatures to achieve reasonable transmission probability, and at those temperatures the quantum isotope effect was small. Recently, we showed that larger, nitrogen-functionalized nanopores could dramatically reduce the barrier height, increasing both the transmission probability at low temperature and the magnitude of the quantum isotope effect.[23] The basic concept of our approach is explained in the next section. Section 3 is dedicated to the quantum chemistry details. On the basis of the obtained potential curves, which are discussed in section 4, we select the most promising candidate for an efficient ^{3}He/^{4}He separation and calculate its overall transmission rate together with the ^{3}He/^{4}He ratio as a function of the temperature in section 5. In section 6, we consider the more realistic situation of a pore size distribution and analyze its effects on the overall performance of the membrane, taking stoichiometric and isomeric variations of the chosen pore structure into account. Finally, in section 7, we examine how the mass-dependence of tunneling and zero-point energy can give rise to a steady-state isotope gradient when a temperature gradient is imposed across the barrier, based on our recent theoretical study in ref 23. The nitrogen-functionalized nanopores studied here show a much greater isotopic enrichment than previously studied structures, so this offers a simple means of isotope separation.

2. THEORY

Because the permeability of a membrane is inversely proportional to its thickness,[24] a one-atom thick sheet of graphene may be considered as the most effective gas separating device possible. If one neglects the role of surface adsorption, the transport of atoms through the membrane reduces to the analysis of the potential barrier a single atom has to overcome when passing through a suitably designed pore with a diameter in the range of a few angstroms. Here, the inclusion of the quantum-mechanical tunneling effect is crucial for a correct prediction of the helium gas transmission. We proceed as follows: First, we determine a suitable form of the tunneling barrier by comparing the transmission functions obtained for a set of analytical benchmark potentials (see section 5 for details on the calculation of the transmission functions). "Suitable" in this context means the potential should provide a low barrier height and have a shape that can be synthesized. Two simple potential functions, a Gaussian peak and a Gaussian peak surrounded by two Gaussian minima, are plotted in Figure 1a. Both analytical functions model the reaction path of a single helium atom passing through a particular graphene pore. For concreteness, a barrier height of 200 cm^{-1} is chosen for both functions, and the minima for the second type are set to −200 cm^{-1} with respect to the asymptotic value of zero energy for infinite distance. In Figure 1b, the corresponding transmission probabilities for ^{3}He and ^{4}He are plotted as functions of the kinetic energy. Two essential features are revealed: (1) The tunneling probability is increased when minima surround the barrier. This is because the deeper minima produce steeper shoulders for the central peak, which narrows the width of the tunneling barrier without reducing the barrier height. Because the wave function decays exponentially inside the classically forbidden region, the barrier narrowing increases the tunneling probability. From a computational standpoint, this also emphasizes the importance of properly accounting for dispersion interactions when computing the potential energy barrier, by using either post-Hartree−Fock methods or
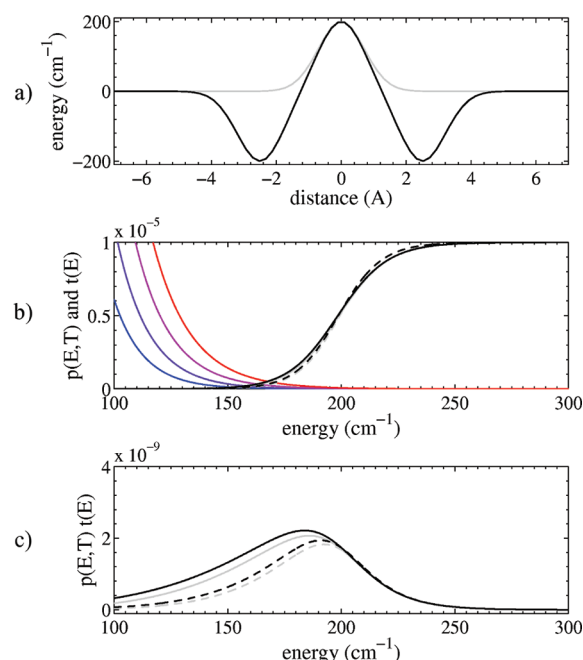

Figure 1. (a) Two possible potential functions (gray and black) for a barrier height of 200 cm^{-1}. In one case, the central peak is surrounded by two minima, which effectively narrow the tunneling barrier by causing steeper shoulders. (b) The corresponding transmission probabilities $t(E)$ (gray and black, almost identical) for ^{3}He (solid lines) and ^{4}He (dashed lines) are plotted together with the kinetic energy distributions $p(E,T)$ (1) for T = 20, 22, 24, and 26 K. Although the transmission functions of both potentials are hardly distinguishable, the product functions $p(E,T)t(E)$ differ. They are printed in (c) for a temperature of T = 20 K. Note that the areas under the solid and dashed curves in (c) are almost equal for the chosen temperature, indicating a ^{3}He/^{4}He transmission ratio, which is already close to 1.

empirical dispersion correction methods. (2) The transmission probabilities in Figure 1b are symmetric in the sense that for low energies ^{3}He is preferred, while at higher energies the tunneling of ^{4}He becomes more likely. For any single-barrier potential, the tunneling probabilities of the two helium isotope coincide when the kinetic energies are the same as the barrier height. Therefore, the selective transmission of ^{3}He is maximized when the kinetic energy of all particles is kept below the barrier height of the potential.

Assuming a Boltzmann distribution for the kinetic energies of the helium atoms, the energy E of a single particle in one dimension for a gas of temperature T is described by a χ^2-distribution with one degree of freedom, which can be written as

$$p(E, T) = \frac{N}{\sqrt{E}}\exp^{-E/k_B T} \tag{1}$$

where N is a normalization factor. This result can be obtained from the better known Gaussian distribution of velocities, v_z.[25] In eq 1, the temperature T is the only parameter that can be used to tune this distribution. From Figure 1b, where four kinetic energy distributions (corresponding to T = 20, 22, 24, and 26 K) are plotted, it can be seen that only with a low barrier height and a sufficiently low temperature does preferential ^{3}He transmission occur. If the kinetic energy distribution declines sufficiently fast, most particles are in the low kinetic-energy range where ^{3}He transmission is favored, whereas only a negligible fraction are in the high-kinetic energy

range where ^{4}He transmission is favored. This can be quantified in terms of $p_w(T)$, the temperature-weighted transmission probability for a single particle, which is obtained by multiplying the kinetic energy distribution $p(E,T)$ with the transmission function $t(E)$ for a given potential, integrated over all possible kinetic energies:

$$p_w(T) = \int p(E, T)t(E)dE \qquad (2)$$

The corresponding product functions for the two chosen potentials are shown Figure 1c for a temperature of $T = 20$ K. From the similar areas under the curves, it can be deduced that the ^{3}He/^{4}He ratio is already close to 1 at 20 K, although ^{3}He is still preferred.

We note that choosing a (classical) Boltzmann distribution for the kinetic energy does not reflect the intrinsic quantum statistical properties of fermionic ^{3}He and bosonic ^{4}He at very low temperatures. However, assuming a Boltzmann distribution for both species avoids the difficulty of treating a mixed, nonideal quantum gas. Besides simplifying the calculation, the Boltzmann distribution provides a more conservative estimate of the ^{3}He/^{4}He transmission selectivity, because the Fermi−Dirac distribution is broader than the Bose−Einstein distribution.

Low temperatures increase the isotope selectivity, but also reduce the transmission probability and hence reduce the total flux rate. Reducing the barrier height increases the transmission probability, but also increases the transmission of high kinetic energy particles, hence reducing the isotope selectivity. For the same reason, higher temperatures with broader kinetic energy distributions necessitate higher barriers. These adjustments have their limits, because the energy distribution becomes more diffuse with increasing temperature and overlaps both the preferentially ^{3}He- and the disadvantageous ^{4}He-transmitting portions of $t(E)$. From a series of tests with several potentials, varying their shape, height, and the gas temperature, we conclude that a barrier of a few hundred wavenumbers, a temperature between 10 and 20 K, and a potential form where the barrier is surrounded by two minima yield the desired effect. While the minima do not noticeably affect the ^{3}He/^{4}He selectivity, their presence improves the overall transmission probability.

To estimate the overall helium flux, the temperature-weighted transmission probability $p_w(T)$ has to be multiplied with the frequency z_{coll} of particle−pore collisions. In the case of Maxwell−Boltzmann distributed gas velocities, this quantity is given by

$$z_{coll} = \rho \langle u \rangle /4 \qquad (3)$$

where ρ denotes the particle density and $\langle u \rangle$ the mean velocity, which is defined as

$$\langle u \rangle = \left(\frac{8k_B T}{\pi m} \right)^{1/2} \qquad (4)$$

Inserting eq 4 into eq 3 and using the ideal gas law to replace ρ by $p/(k_B T)$, one obtains

$$z_{coll} = \frac{p}{\sqrt{2\pi m k_B T}} \qquad (5)$$

with p, m, and k_B denoting the pressure, the atomic mass of the isotopes, and the Boltzmann constant, respectively. Because of the computational demanding evaluation of the potential

energy surface, we consider only one-dimensional transmission through a single least-action path normal to the graphene plane. This provides an upper-bound to the helium flux for two reasons: (1) It assumes that any particle incident upon the surface is transmitted through the pore. Therefore, eq 5 should be reduced by a multiplicative constant to account for the finite cross-sectional area of the pore. (2) It assumes that all incident particles experience a potential energy barrier (and have a transmission probability), which is the same as if they encountered the barrier normal to the plane of the pore. However, the incident atoms have an angular distribution, and the potential energy barriers in these different directions will be wider and higher than the normal-direction reaction coordinate (which corresponds to a minimum potential-energy path). Therefore, $t(E)$ is a function of the collision direction, and in general will be lower than the normal-direction value used here.

We have recently described the thermally driven isotopic enrichment that occurs when two ideal gases at different temperatures are separated by a nanoporous barrier.[23] Although classical barrier transmission cannot lead to any isotopic enrichment, the mass-dependence of tunneling and the zero-point energy at the top of the potential energy barrier give rise to isotope separation. Within a transition-state theory model with tunneling effects, the isotope separation factor is given by

$$r = \frac{(P_{C,4}/P_{C,3})}{(P_{H,4}/P_{H,3})}$$

$$= \left(\frac{p_w^4(T_H)}{p_w^3(T_H)} \right) \left(\frac{p_w^3(T_C)}{p_w^4(T_C)} \right) e^{-(\Delta_3 - \Delta_4)(1/(k_B T_C) - 1/(k_B T_H))} \qquad (6)$$

where $P_{\alpha,i}$ is the partial pressure of isotope i in the compartment having temperature T_α, the p_w^i are computed from eq 2 for each isotope, and Δ_i is the vibrational zero-point energy at the top of the barrier (i.e., of the activated complex). The first two multiplicative terms describe the tunneling contribution, and because $p_w^3(T_\alpha)/p_w^4(T_\alpha) \geq 1$ and is a monotonically decreasing function of temperature (e.g., see Figure 5c), these terms contribute to $r > 1$ (corresponding to enrichment of ^{3}He in the T_H reservoir) so long as $T_C < T_H$. On the other hand, the exponential term describes the zero-point energy effect, and because $\Delta_3 - \Delta_4 > 1$ due to the inverse dependence of vibrational frequencies on particle mass (e.g., consider the quantum harmonic oscillator eigenstates), this term contributes to $r < 1$ (corresponding to enrichment of ^{3}He in the T_C reservoir).

3. QUANTUM CHEMISTRY CALCULATIONS

Having found a suitable shape for the potential barrier function, what atomistic pore structure realizes that function? The simplest case of a graphene pore may be obtained by removing one ring of carbon atoms from the graphene sheet and saturating the carbon atoms with hydrogen atoms where required. This is similar to the interior of the two-dimensional polyphenylene system studied in ref 18. However, the barrier height for this system is 4200 cm^{-1}, and thus from the analysis in section 2, a high ^{3}He/^{4}He transmission ratio occurs only when the helium flux is impractically low. In a systematic study, we therefore increase the pore size, saturating the dangling bonds with hydrogen or nitrogen atoms. The usage of nitrogen for the rim passivation, first proposed in ref 14, allows for a further fine-tuning of the pore size. We found that a

combination of both enlargement strategies provides a sufficiently smooth variation of the overall potential form and allows for a fine-tuning of the crucial tunnel barrier height. Furthermore, this choice of graphene modification reflects ongoing experimental research on the synthesis of nitrogen-doped graphene by chemical vapor deposition,[26] arc-discharge,[27] embedded C and N sources,[28] and post treatments.[29]

We calculated the potential energy barrier using atomistic quantum chemistry calculations based on a finite, molecular model of a single graphene pore. Our model systems consist of the 12/14/15/16 remaining rings in the direct neighborhood for one-, two-, three-, and four-ring-holes, respectively. The model pores are plotted in Figure 2. Because of the size of the
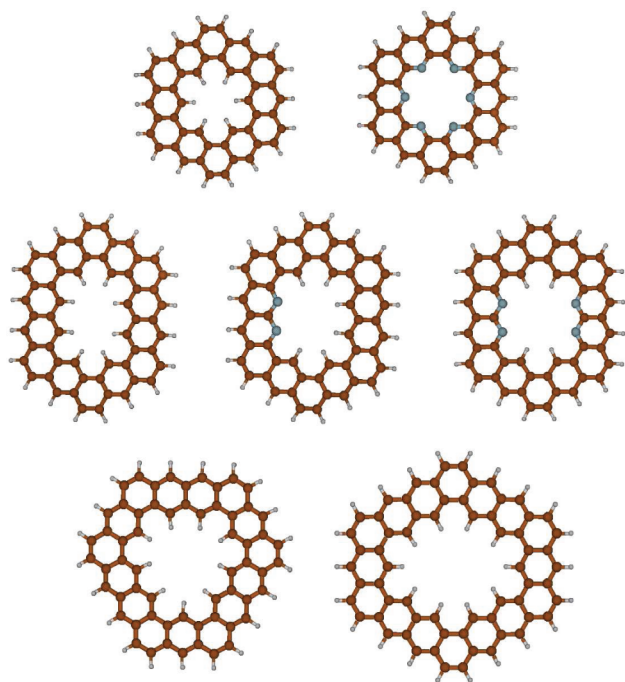

Figure 2. Model systems for the analysis of the helium transmission through a functionalized graphene pore. Single-ring holes are shown in the first row, and the double-ring holes are in the second. A partial replacement of C−H bonds with nitrogen atoms allows for a fine-tuning of the effective pore size. The third row contains a triangular shaped three-ring hole and an even larger four-ring hole. Carbon is printed in orange, hydrogen in white, and nitrogen in blue.

system, ab initio post-Hartree−Fock methods are too computationally demanding; instead we used density-functional theory (DFT) with an empirical dispersion correction. Specifically, we used the B97D functional of Grimme,[30] and a cc-pVTZ triple-ζ basis set[31,32] for all atoms, giving a total of around 2000 contracted Cartesian Gaussian basis functions. Each pore geometry was optimized without helium atoms present. In the subsequent scans for the helium tunneling potential, the geometries for the graphene derivatives were kept frozen. Slight changes in the graphene geometry induced by the transit of a single helium atom are negligibly small ($\Delta E = 6$ cm^{-1} for the single-sided nitrogen-doped pore). All energies are corrected for the basis set superposition error (BSSE) using the method of Boys and Bernardi.[33] We note that the BSSE has its maximum value (typically around 60 cm^{-1}) at the transition state and is of similar size for all pore types. Because of the large

system size, a direct determination of the vibrational frequencies at the transition state is impractical. Instead, we performed single-point calculations in which we moved the He atom in the plane of the pore, and then used the resulting potential energy surface to obtain the vibrational eigenstates. While this neglects the coupling to vibrations of the pore atoms, which would be included in a complete harmonic normal-mode analysis, it more accurately accounts for anharmonic effects. On the basis of our previous calculations of this quantity in other nanoporous systems,[23] the former makes only a small contribution to the total zero-point energy difference, which in practice is much less than the error inherent to the model chemistry. All quantum chemistry calculations were performed using Gaussian 09, revision A02.[34]

4. POTENTIAL BARRIER SIMULATIONS

We start our quest for a suitable pore type with benchmark calculations for small pores, where only one ring has been removed, and try to reduce the barrier height of 4110 cm^{-1} by replacing C−H groups with nitrogen atoms. Although a full nitrogen passivation of such a one-ring-hole reduces its barrier from 4110 to 833 cm^{-1}, this turns out to be still too high for our purpose. Therefore, we enlarge the pore by taking out a second ring, passivating the rim again with hydrogen at first, and we obtain a barrier height of 625 cm^{-1}.

Pores obtained by removing three or more rings made the barrier disappear. However, all but the effectively barrierless largest pores showed the desired feature (see section 2) of a well-developed van der Waals minimum of more than 100 cm^{-1} at a helium distance between 1.9 and 2.5 Å above the pore. Potential curves are given in Figure 3. We note that for all pore
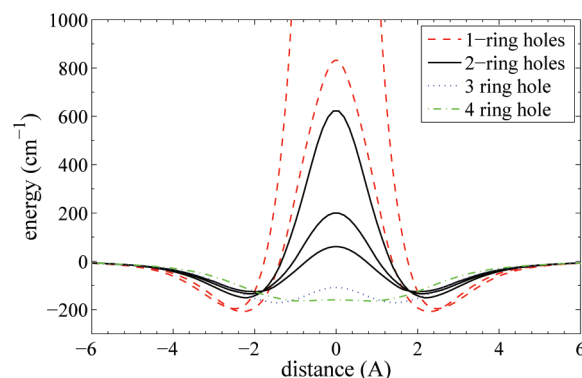

Figure 3. Potential curves for a single helium atom passing through graphene nanopores of different size: single-ring holes (red dashed), two-ring holes (black solid), a triangular three-ring hole (blue dotted), and a large four-ring pore (green dash-dotted). The energy is plotted as a function of the height above the pore perpendicular to the graphene plane. For the single- and double-ring holes, a fine-tuning of the potential barrier by nitrogen passivation of the pore rim is demonstrated. All potentials are corrected for BSSE.

types only the two frequencies describing the in plane-motion of helium are positive; that is, all transition states are first-order saddle points.[35] This is in agreement with the fact that the average pore radii are smaller than 3.70 Å, which is the equilibrium distance of the van der Waals bound HeH dimer in its $^2\Sigma^+$ ground state.[36,37]

Because the barrier height for two-ring holes is close to the desired value, we chose this system for a finer adjustment using hydrogen and nitrogen atoms for the rim passivation. While the

pure hydrogen variant is still too repulsive to provide an acceptable helium flux at low temperature, the barrier almost disappears for a symmetric replacement with four nitrogen atoms; the transition state is found at 61 cm^{-1}. Hence, this pore type, which has been suggested for the separation of methane from hydrogen,[14] does not fulfill the criteria mentioned in section 2. The final adjustment in our approach therefore is to restrict the nitrogen replacement to just one side of the pore. This last step of replacing just two instead of four C–H bonds by nitrogen atoms yields the desired potential form with a barrier height of 201 cm^{-1} and a van der Waals minimum of 134 cm^{-1}. A direct comparison of the pure hydrogen-, the single-sided nitrogen-, and the two-side nitrogen-passivated pore (solid black curves in Figure 3) documents the stepwise adjustment of the barrier height to a suitable value for the separation of ^{3}He from ^{4}He.

Larger pore sizes yield lower barriers. Does (partial) N-passivation of the pore rim introduce additional effects beside those of a simple pore size enlargement? To answer this question, we define "average" pore radii $\langle r \rangle$ for all pores and relate them to the calculated barrier heights. The average radius of a pore is defined as the mean distance between the helium atom position and the van der Waals surfaces of all atoms on the pore rim at the transition state structure. van der Waals radii of 1.10 and 1.55 Å are used for H and N, respectively.[38,39] The obtained pore radii, $\langle r \rangle$, are listed in Table 1, together with the

Table 1. Properties of the Investigated Pore Types: Averaged van der Waals Radius $\langle r \rangle$, Minimum Energy Distance z_{min}, Minimum Energy E_{min}, and Transition State Energy E_{trans}

pore type	$\langle r \rangle$ (Å)	z_{min} (Å)	E_{min} (cm^{-1})	E_{trans} (cm^{-1})	[kcal/mol]
single-ring H-passivated	0.75	2.482	−196	4110	[11.751]
single-ring N-passivated	1.25	2.293	−208	833	[2.382]
two-ring H-passivated	1.48	2.219	−151	625	[1.787]
two-ring single-sided N-passivated	1.57	2.110	−135	201	[0.575]
two-ring two-sided N-passivated	1.68	2.011	−126	61	[0.174]
three-ring H-passivated	1.86	1.447	−171	−108	[−0.309]
four-ring H-passivated	2.25	0.876	−164	−160	[−0.457]

transition state energies, the minimum energies, and the minimum distances for all pores. We use these values in Figure 4 to plot the barrier height divided by the number of rim atoms as a function of $\langle r \rangle$ and apply an exponential fit to the N-free pore types. As expected, we find a good agreement because the barriers are mainly defined by Pauli repulsion. Attractive van der Waals contributions are hardly noticeable on the chosen scale, except for the fact that the barriers change sign for the two largest pores. However, of particular interest is that the N-containing pores do not show any significant deviations from the fitted curve. From this observation, we conclude that nitrogen passivation, at least for the weakly interacting helium, is indeed just another way of pore-size tuning.[40]

From Figure 3, it can be seen that all potential energy barriers relate to a double well potential for symmetry reasons. The bound vibrational states in each of these wells will be split if there is an overlap between the wave functions on the two sides, similar to the tunnel splitting of ammonia. For the numerical calculation of these vibrational eigenstates, we apply a finite difference approach using the reaction paths of Figure 3
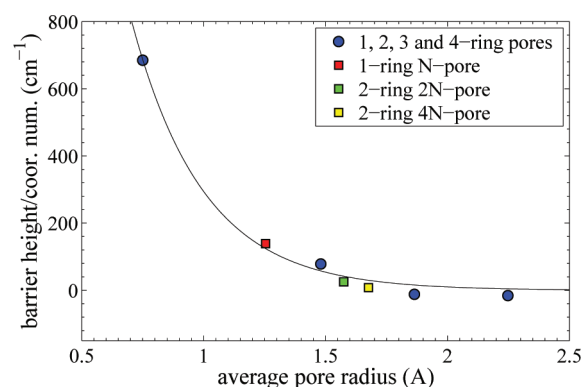

Figure 4. Barrier height divided by the number of rim atoms plotted against the averaged pore radius $\langle r \rangle$ derived from the corresponding pore geometries (see text). The graph proves that the effective pore size is the dominant parameter: A simple exponential fit of the N-free pores reveals that there are no significant deviations for N-containing pores.

as input potentials. The masses of the pore models are set to infinity. Our results for ^{3}He and ^{4}He are summarized in Table 2; the numerical values are only meant to illustrate

Table 2. First Three Vibrational Eigenstates $E_{0,1,2}$ (in cm^{-1}) of ^{3}He and ^{4}He Atoms Attached to the Different Pores^a

pore type	^{3}He			^{4}He		
	E_0	E_1	E_2	E_0	E_1	E_2
single-ring H-passivated	31	89	136	27	78	122
single-ring N-passivated	29	86	134	25	75	119
two-ring H-passivated	26	71	106	23	62	95
two-ring single-sided N-passivated	21	59	91	18	52	81
two-ring two-sided N-passivated	18	53	82	15	46	73
three-ring H-passivated	17	48 (51)	72	15	43 (45)	64
four-ring H-passivated	6	16	32	5	13	27

^{a}The potential minima are referred to as zero energy.

tendencies with regards to pore size variations, because the quantitative values depend strongly on the shape of the potential determined by the model chemistry. The potentials are strongly anharmonic, even for the first few vibrational eigenstates. Tunneling splittings are less than 0.1 cm^{-1} for the single- and the two-ring holes. Only the two reasonably split pairs of eigenstates occurring for the three-ring are included in Table 2. The splitting of the E_1 state is 3.6 cm^{-1} for ^{3}He and 1.7 cm^{-1} for ^{4}He. E_0 splittings of this pore are below one wavenumber, and E_2 already lies above the barrier. The four-ring pore does not show any splitting due to the shallow transition state: even the vibrational ground state lies above the tunneling barrier.

5. MACROSCOPIC QUANTITIES: PARTICLE FLUX AND ^{3}HE/^{4}HE SELECTIVITY

To calculate the ^{3}He and ^{4}He flux from the ab initio potentials, $V(x)$, we apply a Numerov recursion algorithm to solve the time-independent one-dimensional Schrödinger equation:

$$\frac{\delta^2 \psi}{\delta x^2} + \frac{2m}{\hbar^2}(E - V(x))\psi = 0 \qquad (7)$$

for helium atoms with kinetic energies E. The simplification to a one-dimensional description of the tunneling process is justified by the fact that the two in-plane modes of a helium atom are practically unoccupied at low temperatures.[41] Assuming right moving particles of mass m and a sufficiently large discretization interval in x, we can use the asymptotic solutions:

$$\psi(x) = c_t \exp^{ikx} \qquad (8)$$

and

$$\psi(x) = c_i \exp^{ikx} + c_r \exp^{-ikx} \qquad (9)$$

describing free particles ($k = (2mE/\hbar^2)^{1/2}$) far on the right- and the left-hand sides of the barrier, respectively, to obtain the transmission and reflection coefficients from the relations:

$$t = \left|\frac{c_t}{c_i}\right|^2, \; r = \left|\frac{c_r}{c_i}\right|^2 \qquad (10)$$

The Numerov recursion starts on the right-hand side, where c_t, the coefficient of the transmitted wave function, is set to 1 for convenience. The coefficients of the incoming (c_i) and the reflected (c_r) wave function are extracted from the numerical solution on the left side of the interval.[42] A step size of $\Delta x = 0.0125$ Å is chosen for the discretization.

To obtain sufficiently smooth transmission functions $t(E)$, we repeat this procedure for different particle energies E in steps of about 2 cm^{-1}. The temperature dependence is calculated from eq 2. We note that high accuracy in the numerical calculation of the transmission function close to zero energy is essential for obtaining correct results. To be conservative, we set tunneling probabilities of $t(E) < 1 \times 10^{-7}$ to zero, where the numerical solution for quasi-zero energy particles becomes unstable. Because this is in the low kinetic-energy region where ^{3}He is preferentially transmitted, setting these values to zero provides a conservative lower bound of the ^{3}He/^{4}He transmission ratio. Furthermore, to avoid the singularity of the energy distribution in one dimension (see eq 1), we choose the more suitable domain of velocities for the numerical integration to improve the accuracy.

Our results for the single-sided nitrogen-passivated graphene pore are graphically summarized in Figure 5. It contains the (a) thermally weighted transmission of both helium isotopes; (b) ratio of quantum-mechanical to classical transmission; and (c) ^{3}He/^{4}He transmission ratio as a function of the gas temperature. For temperatures below 20 K, both transmission curves in (a) deviate significantly from the classical prediction due to the quantum tunneling of helium atoms. As expected, the transmission of ^{3}He is more likely over the whole temperature range, although above 20 K the ratio approaches 1. In the low temperature regime from 20 to 10 K, the ^{3}He/^{4}He transmission ratio rises from 2 to 19, showing an almost exponential increase. This is a considerable improvement as compared to the performance of the hydrogen-passivated pore (ratio of 3 at 77 K).[18] Besides increasing the ^{3}He selectivity, the main benefit of combining larger pores with low temperatures lies in the much higher transmission probabilities. In the case of the hydrogen-passivated pore, the given ratio has no practical meaning, as it comes only with a negligible transmission
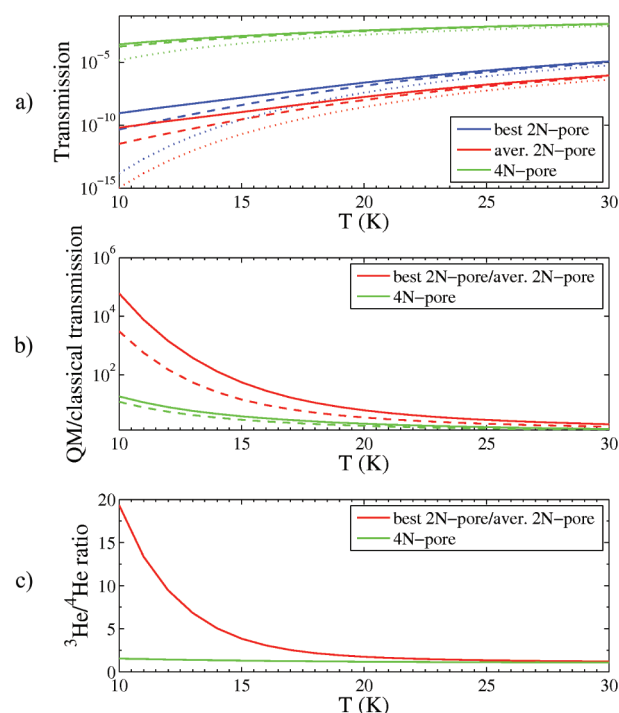

Figure 5. (a) Thermally weighted transmission, eq 2, of ^{3}He (solid lines) and ^{4}He (dashed lines) through a graphene pore (blue, single-sided N-passivated pore; red, isomeric multipore average; green, two-sided N-passivated pore) as a function of temperature. Dotted lines show the corresponding classical transmission probabilities. (b) The ratio of quantum-mechanical to classical transmission probability. (c) The ^{3}He/^{4}He transmission ratio. It drops from 22 to its asymptotic value of 1 within a temperature range of 10 K.

probability below 10^{-36}, providing essentially zero gas flux through the membrane. In contrast, the transmission probabilities for the single-sided nitrogen-passivated pore are in the range of 10^{-9}, allowing for a macroscopic quantity of gas to flow. Following eq 3 to eq 5 and assuming a 100% porous graphene sheet, that is, a theoretical membrane consisting of holes only, ideal gas conditions at 10 K, and a pressure of one bar (collision rate approximately $(3-4) \times 10^{24}$ s^{-1} cm^{-2}), we obtain a total helium flux of more than 10^{-9} moles cm^{-2} s^{-1}, which corresponds to an amount of 3 g helium per day and m^2 of membrane surface.

6. PORE SIZE DISTRIBUTIONS

The helium flux is linearly dependent on the real cross section for a helium-to-hole interaction, and the hole-to-surface ratio will depend on how the pores are assembled into a periodic, two-dimensional sheet. A single-pore-based study does not allow a prediction of this quantity, but it can be used to study effects of pore size distributions. In practice, it may be difficult to synthesize a specific arrangement of nitrogen atoms. To analyze the consequence of inappropriate passivations, we consider all possible variants (at the same stoichiometric ratio). Because of the symmetry of the problem, only 10 out of 28 isomeric pore types are distinguishable. Applying the same quantum chemical approach described above, we obtain the corresponding potential curves and derive the transmission probabilities. Electron density plots for two possible pore types are shown in Figure 6. Replacing C−H bonds on the long sides of the rim increases the effective pore size, while replacement at corner positions does not.[43] Assuming the same probability for
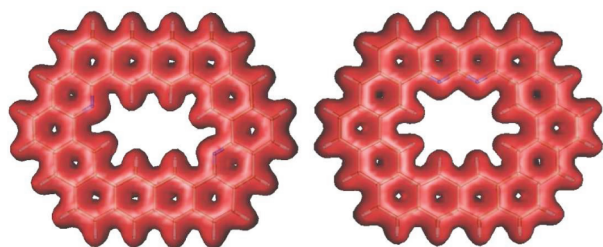
Figure 6. Electron density plots for two possible two-nitrogen passivation variants for the two-ring hole. A relatively high isocontour value of 0.03 electrons per cubic bohr is chosen to emphasize the electron density structure of the pore rim. It can be seen that each replacement of C−H by N breaks one "tooth" out of the hole. Removing two teeth at the same side of the rim (right) leads to the largest and most promising pore type, whereas a replacement in diagonal corners (left) does not increase the effective pore size felt by a helium atom.

each variant to occur,[44] we average over all weighted transmission functions to obtain a more realistic set of curves for Figure 5 (plotted in red). The overall transmission probability decreases by a factor of almost 14, which is the ratio of desired (2) to possible (28) isomeric configurations. Hence, it follows that all other (smaller) pores are quasi-impermeable to helium for the given temperature range due to their higher tunneling barrier. Surprisingly, this does not affect the two ratios plotted in Figure 5b and c. Here, the averaged results coincide almost perfectly with the best-pore ratios and are therefore not distinguishable in the figure. This demonstrates that smaller pores do not interfere with the overall ^{3}He selectivity of the nanoporous graphene sheet, as they are equally impermeable for both isotopes in the given temperature range. The second largest pore type, having the nitrogen atoms on the long sides opposite to each other, yields a barrier height of 256 cm^{-1}, which lies just 55 cm^{-1} above the best pore value. The ^{3}He/^{4}He ratio for this particular pore is 6 at 10 K, but the slightly higher barrier reduces the transmission probabilities for both isotopes by a factor of 10^3. For this reason, the smaller pores do not spoil the average ^{3}He/^{4}He ratio.

However, the situation gets worse when stoichiometric fluctuations in the nitrogen passivation occur. To illustrate the problem, we pick the two-sided N-passivated pore size and calculate the corresponding helium transmissions for this larger pore type. The results are shown in Figure 5 as green curves. For this pore type, the transmission probability is about 10^5 higher, but the ^{3}He/^{4}He selectivity is reduced to only 1.5 at 10 K. As a consequence, the experimental realization of graphene membranes for ^{3}He/^{4}He separation requires a very narrow distribution of pore sizes to keep the membrane selective, or at least must be biased toward pores that are smaller than the desired size. Furthermore, it is advantageous to pick pore types where the largest possible isomeric configuration provides the desired optimum pore size. This is the case for the chosen two-ring-holes with 2-N-passivation.

7. THERMALLY DRIVEN ISOTOPE SEPARATION

We now examine the thermally driven isotope separation factor, eq 6 in high temperature (77−373 K, Figure 7) and low temperature (10−77 K, Figure 8) regimes. The single-ring H-passivated result, shown in Figure S2, is qualitatively similar to the analysis of 2D-PP previously described in ref 23, and the
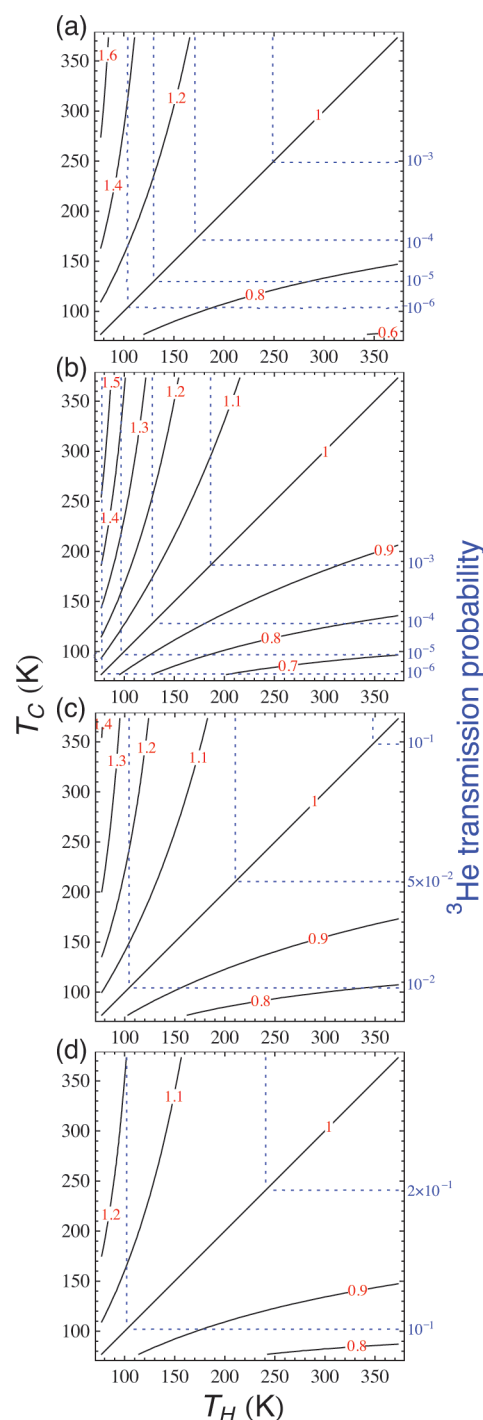

Figure 7. High temperature thermally driven isotope separation factor, eq 6, indicated by black solid contours; blue dotted contours labeled on the right axis indicate the minimum ^{3}He thermally weighted transmission probability, eq 2. (a) Single-ring N-passivated; (b) two-ring H-passivated; (c) two-ring single-sided N-passivated; and (d) two-ring two-sided N-passivated.

primary difference is due to the larger zero-point energy difference, $\Delta_3-\Delta_4$, in the present B97D/cc-pVTZ calculations (68 cm^{-1}) as compared to the previously reported BLYP/6-31G* result (47 cm^{-1}). Because the transmission probabilities are at least 10^9 smaller for that structure, it is not feasible for practical purposes, and we will focus our attention on the larger and nitrogen-substituted pores here. In the high
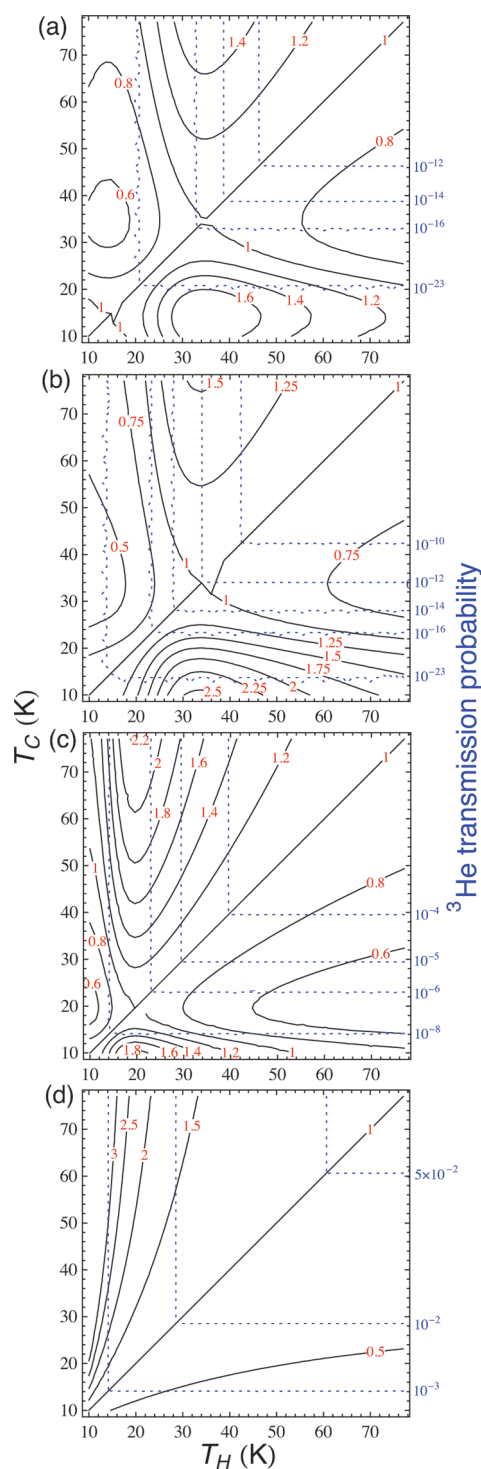
Figure 8. Low temperature thermally driven isotope separation factor, eq 6, following Figure 7. (a) Single-ring N-passivated; (b) two-ring H-passivated; (c) two-ring single-sided N-passivated; and (d) two-ring two-sided N-passivated.

temperature regime, shown in Figure 7, $r < 1$ for $T_C < T_H$ in all cases, indicating that the zero-point energy contributions dominate over tunneling. Taking the modest conditions of an ice−water bath ($T_C = 273$ K) and a boiling water bath ($T_H = 373$ K) to define the two reservoir temperatures, isotope separation factors, r, of 0.94−0.97 are predicted for the four structures shown in Figure 7. In contrast, classical thermodiffusion yields $r = 1.02$ under these conditions;[23] therefore, this

yields a qualitatively different and quantitatively larger isotope effect. The value of r can be further increased by working at lower temperatures: for $T_C = 77$ K (liquid nitrogen temperature) and $T_H = 273$ K, one obtains $r = 0.63$, 0.64, 0.73, and 0.79 for transmission through these four pores. The thermally weighted transmission probabilities even at 77 K are still sufficiently high to make this experiment feasible. Turning to the low temperature regime, shown in Figure 8, we see that some temperature conditions allow for $r > 1$, that is, the dominance of tunneling effects, for all of the pores except for the two-ring two-sided N-passivated species (Figure 8d). However, only the two-ring single-sided N-passivated pore would be practical, because the transmission probabilities for the single-ring N-passivated and two-ring H-passivated pores are both very small in the relevant temperature range. (From Figure 8c, when $T_C = 10$ K and $T_H = 20$ K, $r = 1.86$, and $p_w^3(T_C) = 9 \times 10^{-10}$.) If the goal is to achieve a large isotopic enrichment (regardless of mechanism), then the best option is to use the two-ring two-sided N-passivated pore (Figure 8d), which under these same conditions has a separation factor of $r = 0.34$ (corresponding to a 3:1 isotope enrichment) and a high transmission probability of $p_w^3(T_C) = 2.6 \times 10^{-4}$. However, all of the limitations concerning pore size distribution and isomeric and stoichiometric nitrogen placement discussed in section 6 still apply.

8. CONCLUSION

A partial N-passivation of nanoporous graphene membranes atoms allows for a fine-tuning of the pore size and a stepwise adjustment of the tunneling barrier height to a suitable value for the efficient separation of fermionic ^{3}He from bosonic ^{4}He. Potential barriers for a selection of size-reduced model pore systems were calculated at the B97D/cc-pVTZ level and used to compute the helium transmission probabilities. For a single-pass pressure-gradient driven separation, the highest selectivity is achieved with a two-ring-hole pore type where two C−H bonds on the same side are replaced by nitrogen atoms. We showed that the combination of a large pore size with a very low gas temperature between 10 and 15 K leads to the desired selectivity. The low temperatures keep the kinetic energy distribution of the helium atoms on the low-energy side of the transmission functions, where the tunneling probability for ^{3}He is significantly higher. For a temperature of 10 K, we predict a ^{3}He/^{4}He ratio of 19 at a still acceptable flux of 10^{-9} mol cm^{-2} s^{-1}. With these promising results, an industrial multistage purification of terrestrial helium based on nanoporous graphene membranes seems possible: Assuming a total membrane size of one square meter, this corresponds to a daily production of up to 3 g of ^{3}He . The overall transmission is very sensitive to variations of the pore size, placing high demands upon the experimental realization of a suitably modified graphene sheet. However, the ^{3}He/^{4}He ratio itself is only reduced by contributions from pore sizes larger than the optimum value. Hence, the isotope selectivity can be kept high by choosing systems where the largest-size pore is the optimal barrier, and the other isomers yield smaller (and hence less permeable) pores. We demonstrate that this is the case for the single-sided nitrogen-passivated pore. For the case of a steady-state thermally driven separation, we find that the best results are obtained with a two-ring-hole pore type where four C−H bonds (two on each side) are replaced by nitrogen atoms. Using conditions of $T_C = 10$ K and $T_H = 20$ K, a 1:3 isotopic enrichment is possible, and the transmission probability is

$>10^{-4}$, allowing the system to reach a steady state at an experimentally reasonable rate. While the current work considers only single-barrier tunneling, in principle resonant tunneling through multilayers could offer improved flux and isotope selectivity. We are currently investigating methods of aligning nanoporous graphene multilayers to determine the extent of this enhancement.

■ ASSOCIATED CONTENT

ⓢ Supporting Information

Optimized geometries for the two-ring pores (H-passivated, single-sided N-passivated, and two-sided N-passivated) in Cartesian coordinates. Comparison of all isomeric configurations of the single-sided N-passivated pore. Plot of the thermally driven isotope separation across the single-ring H-passivated pore, and plot of the quantum-tunneling-only thermally driven isotope separation across the single-ring N-passivated and two-ring pores. This material is available free of charge via the Internet at http://pubs.acs.org.

■ AUTHOR INFORMATION

Corresponding Author

*E-mail: andreas.w.hauser@gmail.com (A.W.H.); jschrier@haverford.edu (J.S.); peter.schwerdtfeger@gmail.com (P.S.).

Notes

The authors declare no competing financial interest.

■ ACKNOWLEDGMENTS

■ REFERENCES

(1) Cho, A. *Science* **2009**, *326*, 778−779.

(2) Hauser, A.; Schwerdtfeger, P. *J. Phys. Chem. Lett.* **2012**, *3*, 209−213.

(3) Novoselov, K. S.; Geim, A. K.; Morozov, S. V.; Jiang, D.; Zhang, Y.; Dubonos, S. V.; Grigorieva, I. V.; Firsov, A. A. *Science* **2004**, *306*, 666−669.

(4) Avouris, P.; Chen, Z.; Perebeinos, V. *Nat. Nanotechnol.* **2007**, *2*, 605−615.

(5) Geim, A. K.; Novoselov, K. S. *Nat. Mater.* **2007**, *6*, 183−191.

(6) Beenakker, C. W. J. *Rev. Mod. Phys.* **2008**, *80*, 1337−1354.

(7) Castro Neto, A. H.; Guinea, F.; Peres, N. M. R.; Novoselov, K. S.; Geim, A. K. *Rev. Mod. Phys.* **2009**, *81*, 109−162.

(8) Park, S.; Ruoff, R. S. *Nat. Nanotechnol.* **2009**, *4*, 217−224.

(9) Bonaccorso, F.; Sun, Z.; Hasan, T.; Ferrari, A. C. *Nat. Photonics* **2010**, *4*, 611−622.

(10) Bunch, J. S.; Verbridge, S. S.; Alden, J. S.; van der Zande, A. M.; Parpia, J. M.; Craighead, H. G.; McEuen, P. L. *Nano Lett.* **2008**, *8*, 2458−2462.

(11) Leenaerts, O.; Partoens, B.; Peeters, F. M. *Appl. Phys. Lett.* **2008**, *93*, 193107.

(12) Fischbein, M. D.; Drndic, M. *Appl. Phys. Lett.* **2008**, *93*, 113107−1−3.

(13) Kuhn, P.; Forget, A.; Su, D.; Thomas, A.; Antonietti, M. *J. Am. Chem. Soc.* **2008**, *130*, 13333−13337.

(14) en Jiang, D.; Cooper, V. R.; Dai, S. *Nano Lett.* **2009**, *9*, 4019−4024.

(15) Li, Y.; Zhou, Z.; Shen, P.; Chen, Z. *Chem. Commun.* **2010**, *46*, 3672−3674.

(16) Blankenburg, S.; Bieri, M.; Fasel, R.; Müllen, K.; Pignedoli, C. A.; Passerone, D. *Small* **2010**, *6*, 2266−2271.

(17) Jiao, Y.; Du, A.; Hankel, M.; Zhu, Z.; Rudolph, V.; Smith, S. C. *Chem. Commun.* **2011**, *47*, 11843−11845.

(18) Schrier, J. *J. Phys. Chem. Lett.* **2010**, *1*, 2284−2287.

(19) Sint, K.; Wang, B.; Král, P. *J. Am. Chem. Soc.* **2008**, *130*, 16448−16449.

(20) Garaj, S.; Hubbard, W.; Reina, A.; Kong, J.; Branton, D.; Golovchenko, J. A. *Nature* **2010**, *467*, 190−193.

(21) Suk, M. E.; Aluru, N. R. *J. Phys. Chem. Lett.* **2010**, *1*, 1590−1594.

(22) Hankel, M.; Jiao, Y.; Du, A.; Gray, S. K.; Smith, S. C. *J. Phys. Chem. C* **2012**, *116*, 6672−6676.

(23) Schrier, J.; McClain, J. *Chem. Phys. Lett.* **2012**, *521*, 118−124.

(24) Oyama, S.; Lee, D.; Hacarlioglu, P.; Saraf, R. *J. Membr. Sci.* **2004**, *244*, 45−53.

(25) The "unexpected" $E^{-1/2}$ dependence of $p(E,T)$ is an artifact of the 1D-representation and assures that the total kinetic energy in three dimensions is Boltzmann-distributed.

(26) Wei, D.; Liu, Y.; Wang, Y.; Zhang, H.; Huang, L.; Yu, G. *Nano Lett.* **2009**, *9*, 1752−1758.

(27) Panchakarla, L. S.; Subrahmanyam, K. S.; Saha, S. K.; Govindaraj, A.; Krishnamurthy, H. R.; Waghmare, U. V.; Rao, C. N. R. *Adv. Mater.* **2009**, *21*, 4726−4730.

(28) Zhang, C.; Fu, L.; Liu, N.; Liu, M.; Wang, Y.; Liu, Z. *Adv. Mater.* **2011**, *23*, 1020−1024.

(29) Wang, X.; Li, X.; Zhang, L.; Yoon, Y.; Weber, P. K.; Wang, H.; Guo, J.; Dai, H. *Science* **2009**, *324*, 768−771.

(30) Grimme, S. *J. Comput. Phys.* **2006**, *27*, 1787−1799.

(31) Dunning, T. H. J. *J. Chem. Phys.* **1989**, *90*, 1007−1023.

(32) Woon, D. E.; Dunning, T. H. J. *J. Chem. Phys.* **1994**, *100*, 2975−2988.

(33) Boys, S. F.; Bernardi, F. *Mol. Phys.* **1970**, *19*, 553−566.

(34) Frisch, M. J.; Trucks, G. W.; Schlegel, H. B.; Scuseria, G. E.; Robb, M. A.; Cheeseman, J. R.; Scalmani, G.; Barone, V.; Mennucci, B.; Petersson, G. A.; et al. *Gaussian 09*, revision A.02; Gaussian, Inc.: Wallingford, CT, 2009.

(35) The four-ring hole still shows a (very shallow) first-order saddle point. This feature is significantly enhanced by the BSSE correction, but is also still present on the uncorrected potential surface.

(36) Theodorakopoulos, G.; Petsalakis, I. D.; Nicolaides, C. A.; Buenker, R. J. *J. Phys. B: At. Mol. Phys.* **1987**, *20*, 2339.

(37) Theodorakopoulos, G.; Farantos, S. C.; Buenker, R. J.; Peyerimhoff, S. D. *J. Phys. B: At. Mol. Phys.* **1984**, *17*, 1453.

(38) Bondi, A. *J. Phys. Chem.* **1964**, *68*, 441−451.

(39) Rowland, R. S.; Taylor, R. *J. Phys. Chem.* **1996**, *100*, 7384−7391.

(40) We note that a correction of helium-to-rim distances via atomic van der Waals radii is essential. Treating N and H as point particles is an oversimplification that leads to significant deviations for the N-containing pores, which would be contradictory to our conclusion.

(41) For example, for the single-sided N-passivated pore, we obtain 118 and 201 cm^{-1} (72 and 164 cm^{-1} without BSSE correction) for the in-plane modes.

(42) A detailed description of this standard approach is given in ref 45, where a third-order finite difference method is used. Numerov's recursion is of fourth order.

(43) Interestingly, for the three possible (distinguishable) corner-only 2-N-passivations, we find even higher tunneling barriers than for the pure H-passivated pore. Nitrogen atoms on corner positions allow for a slight rearrangement of the model pore, which leads to a more compact structure with a tendency to interlocked C−H teeth.

(44) The real size distribution depends on the mechanism used for creating the pores. Thermodynamically, the smaller pores, having the two nitrogen atoms well separated from each other, tend to be more favorable. Pore arrangements with the two nitrogen atoms in direct neighborhood provide larger holes but are higher in energy (see the Supporting Information).

(45) Cedillo, A. *J. Chem. Educ.* **2000**, *77*, 528−531.